1-1-2021

Dynamical Comparison of Different Polymer Architectures - Bottlebrush vs Linear Polymer

Karin J. Bichler
Louisiana State University

Bruno Jakobi
Louisiana State University

Gerald J. Schneider
Louisiana State University

Recommended Citation

Bichler, K., Jakobi, B., & Schneider, G. (2021). Dynamical Comparison of Different Polymer Architectures - Bottlebrush vs Linear Polymer. *Macromolecules* https://doi.org/10.1021/acs.macromol.0c02104

Macromolecules

pubs.acs.org/Macromolecules Article

Dynamical Comparison of Different Polymer Architectures—Bottlebrush vs Linear Polymer

Karin J. Bichler,* Bruno Jakobi, and Gerald J. Schneider*

Cite This: *Macromolecules* 2021, 54, 1829–1837 Read Online

ACCESS | Metrics & More | Article Recommendations | Supporting Information

ABSTRACT: Different polymer architectures behave differently regarding their dynamics. We have used a combination of dielectric spectroscopy, and fast field cycling nuclear magnetic resonance (NMR) to compare the dynamical behavior of two different polymer architectures, with similar overall molecular weight. The systems of interest are a bottlebrush polymer and a linear one, both based on poly(dimethylsiloxane) (PDMS). To verify the structure of the PDMS-g-PDMS bottlebrush in the melt, small-angle neutron scattering was used, yielding a spherical shape. Information about the segmental dynamics was revealed by dielectric spectroscopy and extended to higher temperatures by fast field cycling NMR. One advantage of fast field cycling NMR is the detection of large-scale chain dynamics, which dielectric spectroscopy cannot probe for PDMS. While segmental relaxation seems to be independent of the architecture, the large-scale chain dynamics show substantial differences, as represented by the mean square displacement. Here, two regions are detected for each polymer. The linear polymer shows the Rouse regime, followed by reptation. In contrast, the bottlebrush polymer performs Rouse dynamics and diffusion in the available time window, and entanglement effects are completely missing.

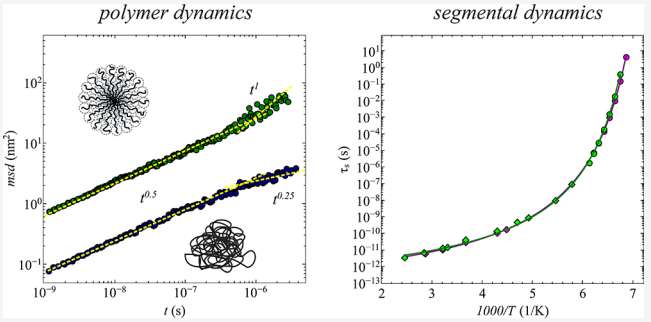

INTRODUCTION

Properties of polymers strongly depend on the architecture as well as on the molecular weight. This includes the material as well as the dynamical behavior.[1−3] One architecture of interest are bottlebrush polymers, i.e., linear side chains covalently bonded on a linear backbone. This type of polymer is highly customizable regarding its shape,[4−7] chemical composition,[4,5,8,9] and grafting density,[10,11] i.e., number of side chain per backbone unit, and received great interest in recent times. Due to their versatility, several applications are known, like supersoft elastomers, drug delivery agents, or viscoelasticity modifiers.[12−14] Since linear side chains are chemically attached to the backbone, bottlebrushes show extraordinary rheological properties, connected to a shift of entanglement molecular weight to higher values, which are the main focus of research so far.[9,10,15,16] Regarding their dynamical behavior, bottlebrush polymers show a hierarchical relaxation process, whereby the outermost segments relax at first, while the segments close to the branching point relax at a later time, followed by the bottlebrush polymer itself.[8,15,17] Similar relaxation behavior can be tracked by dielectric spectroscopy via the segmental relaxation for bottlebrushes. Hereby, a slowed-down process of the segmental relaxation depending on the sidechain length was found, by comparing the bottlebrush polymers with their respective single side chains. This supports a hierarchical relaxation pattern of the bottlebrush polymer based on the segmental relaxation.[4,18] As reported by López-Barrón et al., the intermolecular correlation decreases with increasing sidechain length, which influences the α-relaxation. This results in less backbone contribution on the relaxation for longer side chains, giving further support for the characteristic relaxation behavior of bottlebrush polymers.[19]

In this publication, we are focusing on a comparison of poly(dimethylsiloxane) (PDMS)-based polymers with different architectures, i.e., PDMS-g-PDMS bottlebrush vs linear PDMS, both having similar overall molecular weight. This gives insight into how the dynamical behavior changes if the repeating units are arranged differently, based on the morphology. Since PDMS is one of the most flexible polymers, it is very suitable for dynamical studies, regarding segmental relaxation and polymer dynamics. The spherical shape of our bottlebrush polymer in the melt state was confirmed by small-angle neutron scattering (SANS), while for the dynamical investigations, a combination of dielectric spectroscopy (DS) and fast field cycling (FFC) nuclear magnetic resonance (NMR) was used. With dielectric spectroscopy, information about the

Received: September 11, 2020
Revised: January 18, 2021
Published: February 3, 2021

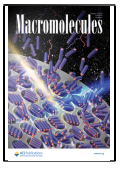

https://dx.doi.org/10.1021/acs.macromol.0c02104
Macromolecules 2021, 54, 1829−1837

segmental dynamics of PDMS are obtained, since PDMS is classified as a type B polymer with a permanent dipole moment perpendicular to the main chain.[20] In contrast, FFC-NMR has access to both the segmental dynamics and polymer dynamics. While the segmental dynamics can be combined with those of dielectric spectroscopy, for polymer dynamics, it is very convenient to focus on the mean square displacement, $\langle r^2(t)\rangle$, to identify different dynamical processes and compare them over the two samples.

THEORETICAL BACKGROUND

Small-Angle Neutron Scattering. Small-angle neutron scattering data of the PDMS-g-PDMS bottlebrush melt have been analyzed by a spherical core−shell form factor, $P(Q)$, including an explicit density profile as used for star polymers, $\varphi_{star}(r)$, and blob contribution, accounting for internal shell density fluctuations. Due to the negligible core size, the core contribution was excluded in the model function and our bottlebrush can be seen as a star polymer. The detailed form factor, $P(Q)$, has previously been published in Bichler et al.[5] for a similar sample system.

Our PDMS-g-PDMS bottlebrush sample has been measured in a complete melt state with isotopic labeling, i.e., a mixture of protonated ((h-PDMS)-g-(h-PDMS)) and deuterated ((h-PDMS)-g-(d-PDMS)) bottlebrushes. Since the degree of polymerization of both bottlebrushes is slightly different, the random phase approximation (RPA)[21]

$$\frac{(\Delta\rho)^2}{I(Q)} = \frac{1}{\Phi_{BB_h} V_{BB_h} \tilde{P}(Q)_{BB_h}} + \frac{1}{\Phi_{BB_d} V_{BB_d} \tilde{P}(Q)_{BB_d}} - \frac{2\chi}{V_0} \tag{1}$$

with the modified form factors $\tilde{P}(Q)_{BB_i}$ for the deuterated and protonated PDMS-g-PDMS bottlebrush polymers

$$\tilde{P}(Q)_{BB_i} = A(Q)^2_{shell_i} \frac{1}{f_i}(f_i - 1) + a_i \cdot \frac{1}{f_i} P(Q)_{blob_i} \tag{2}$$

according to Bichler et al.[5] has been used. The volume of the bottlebrushes is calculated as

$V_{BB_i} = f_i \cdot \frac{M_{w_i}^{side\ chain}}{\varrho_i N_A}$ with the number of side chains, f_i, the weight average molecular weight of the side chains, $M_{w_i}^{side\ chain}$, and the mass density, ϱ_i, of the respective bottlebrush polymers together with the Avogadro constant, N_A. Furthermore, Φ_{BB_i} denotes the volume concentration of the two differently labeled bottlebrush polymers, and $V_0 = \sqrt{V_h V_d}$ is the geometric average monomer volume with V_h and V_d being the protonated and deuterated monomer volumes, respectively. The Flory−Huggins interaction parameter, χ, describes the miscibility behavior of the two polymers in the mixture. The scattering amplitudes of the shell, $A(Q)_{shell_i}$, and the blob contribution, $P(Q)_{blob_i}$, have been used as previously published.[5] Due to the melt state of the sample, we have a Θ-condition connected to the Flory exponent of $\nu = 0.5$, as used for the data modeling.

Dielectric Spectroscopy. Dielectric spectroscopy measures the fluctuations of the permanent dipole moment depending on the applied electric field, $E(t)$. PDMS has only a permanent dipole moment perpendicular to the polymer main chain and thus classified as a type B polymer. Therefore, dielectric spectroscopy only tracks the segmental dynamics, i.e., the α-relaxation.[20]

The simplest description for a relaxation process is using the Debye approach with τ_D as the characteristic relaxation time of the system.[20,22]

$$\varepsilon^*(\omega) = \varepsilon_\infty + \frac{\Delta\varepsilon}{1 + i\omega\tau_D} \tag{3}$$

However, nonideal processes cannot be described using eq 3 due to asymmetric shapes that are not accounted for in the Debye model. Usually, the empirical Havriliak−Negami (HN) function is used for describing nonexponential relaxation processes

$$\varepsilon^*_{HN}(\omega) = \varepsilon_\infty + \frac{\Delta\varepsilon}{(1 + (i\omega\tau_D)^\beta)^\gamma} \tag{4}$$

with the two shape parameters β and γ accounting for the asymmetric broadening of the relaxation spectra. These two parameters need to follow the restrictions of $0 < \beta \leq 1$ and $0 < \beta\gamma \leq 1$, which describe the slopes of the low- and high-frequency side of the relaxation peak.[20]

The relaxation time associated with the peak maximum of the relaxation process is determined by[4,23]

$$\frac{1}{\tau_s} = \frac{1}{\tau_{HN}}\left[\sin\left(\frac{\beta\pi}{2 + 2\gamma}\right)\right]^{1/\beta}\left[\sin\left(\frac{\beta\gamma\pi}{2 + 2\gamma}\right)\right]^{-1/\beta} \tag{5}$$

and the temperature behavior can be described with the Vogel−Fulcher−Tammann (VFT) equation

$$\tau_s = \tau_\infty \exp\left(\frac{A}{T - T_0}\right) \tag{6}$$

with τ_∞ being the limiting relaxation time for infinitely high temperatures, T_0 being the ideal glass transition temperature, and A being a constant.

Fast Field Cycling Relaxometry. Fast field cycling relaxometry measures the Larmor frequency dependence of the spin-lattice relaxation rate, $R_1(\omega) = \frac{1}{T_1(\omega)}$, by rapidly switching (cycling) the external magnetic detection field, whereby $T_1(\omega)$ stands for the spin-lattice relaxation time. Here, $\omega = -\gamma_H B_0$ is the Larmor frequency with γ_H the gyromagnetic ratio of the protons and B_0 the experimentally controlled external magnetic field, the sample is exposed to.[24]

The measured relaxation rate is composed of intra- and intermolecular parts, $R_1(\omega) = R_1^{intra}(\omega) + R_1^{inter}(\omega)$. Intramolecular relaxation is attributed to segmental reorientation dynamics, whereas the intermolecular part describes translational motions of segments from different molecules. Since $R_1^{inter}(\omega)$ is connected to polymer dynamics at low fields, it allows to derive the mean square displacement, $\langle r^2(t)\rangle$.[24,25]

The relaxation rate, $R_1(\omega)$, can be written by the Bloemberg−Purcell−Pound (BPP) equation

$$R_1(\omega) = K[J_{DD}(\omega) + 4J_{DD}(2\omega)] \tag{7}$$

with the dipolar spectral density, $J_{DD}(\omega)$, and the dipolar coupling constant, K. Multiplication of $J_{DD}(\omega)$ with ω yields the dynamic susceptibility, $\chi''(\omega) = \omega J_{DD}(\omega)$, and allows to rewrite the BPP equation to

$$\omega R_1(\omega) = K[\chi''(\omega) + 2\chi''(2\omega)] \cong 3K\chi''_{FC}(\omega) \tag{8}$$

https://dx.doi.org/10.1021/acs.macromol.0c02104
Macromolecules 2021, 54, 1829−1837

Assuming that K does not significantly change with temperature, the dipolar susceptibility, $\omega R_1(\omega) = \chi''_{DD}(\omega)$, can be introduced, allowing to obtain the susceptibility master curves. The evolving relaxation peak can be described with the Cole–Davidson (CD) function[20]

$$\chi''_{DD}(\omega) = K[\mathrm{CD}(\omega) + 2\mathrm{CD}(2\omega)] \tag{9}$$

resulting in the relaxation time, τ_{CD}, associated with the respective reference temperature, T_{ref}, of the master curve.[24,26] This time needs to be corrected for the shape parameter, γ, by

$$\frac{1}{\tau_s} = \frac{1}{\tau_{CD}}\tan\left(\frac{\pi}{2+2\gamma}\right) \tag{10}$$

Using the suitable shift parameter, a_T, used for creating the susceptibility master curve, enables to obtain the relaxation times of the other measured temperatures.

The mean square displacement, $\langle r^2(t)\rangle$, is connected via a cosine transformation with the intermolecular relaxation rate, $R_1(\omega)$, and can be derived by

$$\langle r^2(t)\rangle = \frac{1}{2}\left[\frac{5}{4}\left(\frac{4\pi}{\mu_0}\right)^2\sqrt{\frac{8}{3\pi^3}}\frac{1}{\gamma_H^4\hbar^2 n_s}\frac{1}{1+2^{1+3\alpha/2}}\int_0^\infty R_1^{inter}(\omega)\cos(\omega t)\mathrm{d}\omega\right]^{-2/3} \tag{11}$$

with the spin density, n_s, the magnetic constant, μ_0, and $\alpha \in [0.25;1]$ based on the underlying polymer dynamics.[24,26]

In the case of PDMS, the intermolecular relaxation rate, $R_1^{inter}(\omega)$, is directly obtained from purely protonated samples for $\omega < \tau_s^{-1}$. For higher fields, the intramolecular relaxation rate, $R_1^{intra}(\omega)$, is dominating, resulting in relaxation times of the segmental dynamics.[25,26]

EXPERIMENTAL SECTION

Samples. The bottlebrush polymers were synthesized based on the grafting-to method, via the reaction of living PDMS chains, obtained by kinetically controlled anionic ring-opening polymerization of hexamethylcyclotrisiloxane, with a chlorinated backbone as illustrated in Scheme 1 and published in Bichler et al.[5] The molecular parameters based on gel-permeation chromatography-multi-angle laser light scattering (GPC-MALLS) of the protonated, deuterated bottlebrushes and the linear polymer are summarized in Table 1.

Scheme 1. Synthetic Scheme toward PDMS Bottlebrushes via a Grafting-to Method of Living PDMS Chains onto Polychloromethylsiloxane[5]

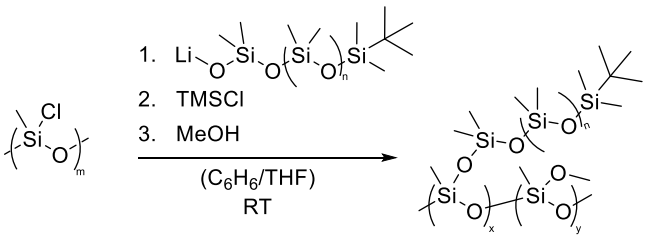

Small-Angle Neutron Scattering. Small-angle neutron scattering experiments were conducted on the NGB30m SANS instrument at the National Institute of Standard and Technology Center for Neutron Research (NIST-NCNR), Gaithersburg, MD.[27] Three different sample-to-detector distances, d = 1.3, 4.0, and 13.1 m together with a wavelength of λ = 6 Å with $\Delta\lambda/\lambda$ = 13.8%, offered a Q-range of 0.003 Å^{-1} < Q < 0.47 Å^{-1} with the momentum transfer, $Q = \frac{4\pi}{\lambda}\sin\left(\frac{\vartheta}{2}\right)$, and scattering angle, ϑ. The data reduction was performed using the suite of NCNR SANS reduction macros in the IGOR software package (WaveMetrics, Portland, OR).[28]

Table 1. Weight Average Molecular Weight, M_w, Number Average Molecular Weight, M_n, Degree of Polymerization, DP, and M_w/M_n, for the Protonated Bottlebrush, (h-PDMS)-g-(h-PDMS), the Deuterated Bottlebrush, (h-PDMS)-g-(d-PDMS), and the Linear PDMS, PDMSlin380k. Number of side chains, f, and grafting density, z, for the protonated, (h-PDMS)-g-(h-PDMS), and the deuterated bottlebrush, (h-PDMS)-g-(d-PDMS).

	M_w (g/mol)	M_n (g/mol)	DP	M_w/M_n	f	z
		(h-PDMS)-g-(h-PDMS)				
side chain	8900	8100	110	1.10		
backbone	4230	4160	70	1.02		
bottlebrush	431 000	385 000		1.12	47	0.67
		(h-PDMS)-g-(d-PDMS)				
side chain	11 400	10 800	136	1.07		
backbone	4230	4160	70	1.02		
bottlebrush	446 000	404 000		1.10	37	0.53
		PDMSlin380k				
linear PDMS	380 000	370 000	5135	1.03		

Dielectric Spectroscopy. Dielectric spectroscopy experiments were performed with a Broadband Dielectric Alpha Analyzer from Novocontrol GmbH in a frequency range of 10^{-2}–10^6 Hz. A temperature range of T = −140.0 to −90.0 °C was enough to shift the segmental dynamic through the available frequency window. The temperature was controlled by a Quatro Cryosystem having a manufacturer specified accuracy of 0.1 °C. For ensuring temperature equilibrium prior to the measurement, an equilibration time of 3 min was used. Since PDMS is a semicrystalline polymer with a great tendency for crystallization, the samples were rapidly cooled to T = −140.0 °C to minimize crystallization during the measurements. Therefore, each sample was measured from low to high temperatures.

Fast Field Cycling Relaxometry. The fast field cycling relaxometry experiments were performed on the SMARTracer FFC-NMR from STELAR. It consists of a B = 0.25 T electromagnet, offering a measurable Larmor frequency range of 10 kHz–10 MHz. Minimizing external influences, by increasing the distance between the electric control unit and the electromagnet by 1.5 m together with removing of magnetizable parts as far as possible, shifts the lower limit to 5 kHz. For the samples investigated here, a temperature range of T = −100 to +135 °C was used to create the master curves including the relaxation peak associated with the segmental relaxation. Prior to each scan, the samples were quenched in liquid nitrogen to minimize crystallization during the measurement.

RESULTS AND DISCUSSION

Structural Analysis—Small-Angle Neutron Scattering. Small-angle neutron scattering experiments have been performed on a blend of isotopically labeled bottlebrush polymers, based on PDMS. A low concentration, Φ = 0.5%, of protonated, (h-PDMS)-g-(h-PMDS), in deuterated, (h-PDMS)-g-(d-PDMS), bottlebrushes gives access to the pure form factor of the protonated species, as illustrated in Figure 1.

Here, a direct transition from low (Guinier region) to intermediate Q's (Porod region) is visible, with an intensity dependence of $Q^{-4.0}$ in the Porod region. Continuing to larger momentum transfers, i.e., Q > 0.1 Å^{-1}, the so-called blob

https://dx.doi.org/10.1021/acs.macromol.0c02104
Macromolecules 2021, 54, 1829–1837

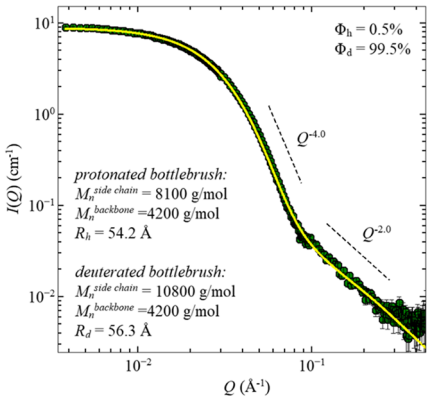

Figure 1. Scattering intensity, $I(Q)$, vs momentum transfer, Q, for a low concentration, $\Phi = 0.5\%$, of protonated, (h-PDMS)-g-(h-PDMS), in deuterated, (h-PDMS)-g-(d-PDMS), bottlebrush polymers, taken at room temperature. The dashed lines indicate the power law dependence of the intensity. The solid line is the best description by the form factor using eq 1.

region emerges, showing a power law dependence, Q^{-d_f}, with $d_f = 2.0$. For our sample, the overall structure is identified as compact spherical and can be well described using the random phase approximation (RPA) with the core−shell form factor as introduced in eq 1. Hereby, the parameters for the deuterated specie were kept constant at those values reported in Bichler et al.[5] for the deuterated PDMS-g-PDMS bottlebrush polymer immersed in a linear PDMS matrix with $M_n = 8700$ g/mol.

The high Q region describes the chain conformation within the bottlebrush shell. Due to the inverse proportionality of the slope in the blob region to the Flory exponent, ν, i.e., $d_f \propto -1/\nu$, the solvent quality for the protonated PDMS-g-PDMS bottlebrush can be determined.[5,29] In our case, the blob region shows a well-pronounced Q^{-2} dependence leading to $\nu = 0.5$, which is suitable for Θ- or melt condition made up by the deuterated bottlebrushes. The description of this region is included in the model function and results in the blob size, ξ, which is assumed to be equal for all blobs of the side chains based on scaling theory.[30] The blob represents a size range, where the grafted polymer behaves as a free, unperturbed polymer chain.

The resulting fit parameters for the protonated and the deuterated PDMS-g-PDMS bottlebrush polymers are summarized in Table 2.

Comparing the two radii of the protonated, R_h, and the deuterated, R_d, species, the latter one shows a larger value, which is accompanied with the higher degree of polymerization of the side chains. In this case, the side chains are longer compared to the protonated version, thus the greater radius. While concentrating on the blob size, our results imply a possible correlation with the grafting density, which is represented as the number of side chains. As higher the grafting density, as closer the side chains are located compared to their next neighbors; thus, the resulting blob size may decrease. This could explain the smaller blob size, in the case of the protonated species, due to the higher grafting density compared to the deuterated one. Another interesting result of the model description is the Flory−Huggins interaction parameter, χ, which describes the miscibility behavior of polymer blends.[31] Based on the analysis, the interaction parameter shows a value of $\chi = 0.00024$, suitable for very similar components within the polymer blend.[32] This result

Table 2. Resulting Fit Parameters for the Protonated and Deuterated Bottlebrush Polymers, (h-PDMS)-g-(h-PDMS) and (h-PDMS)-g-(d-PDMS), Together with the Calculated Scattering Length Density (SLD)[a]

parameter	(h-PDMS)-g-(h-PDMS)	(h-PDMS)-g-(d-PDMS)
overall radius R (Å)	54.2	56.3
number of side chains f	47	39
blob size ξ (Å)	9.0	14.2
scaling parameter of blob a	0.12	0.14
smearing parameter σ	0.36	0.36
Flory−Huggins interaction parameter χ	0.00024	
scattering length density (SLD) (cm^{-2})	6.74×10^8	3.28×10^{10}

[a]Standard deviations are <1%.

seems reasonable since the only major difference in the blend is the different isotopic labeling.

Dynamics. *Segmental Dynamics—Dielectric Spectroscopy.* Figure 2a and b illustrate the dielectric permittivity, ε'', as a function of frequency, f, for different temperatures, ranging from $T = -125.0$ to -90.0 °C for the PDMS-g-PDMS bottlebrush polymer.

With increasing temperature, the relaxation peak moves to higher frequencies, associated with a decreasing relaxation time. Furthermore, the peak height decreases with temperature. At a certain temperature, $T = -107.5$ °C, the first relaxation process is substituted by a second process, possessing the same behavior, i.e., with increasing temperature, the peak maximum shifts to higher frequencies. PDMS is known to show two processes, both belonging to the segmental relaxation and routed in the same origin, i.e., the permanent dipole moment.[4,33]

While at very low temperatures, the pure segmental relaxation, i.e., the α-relaxation, is observable, increasing temperature leads to the second process, the α_c-relaxation. The latter phenomenon arises from the emerging crystallization, due to the semicrystallinity of PDMS, and describes a slowed-down segmental relaxation due to the formation of crystallites.[4,33] Therefore, the abbreviation α_c is used.

Translated to our sample, the first process, Figure 2a, describes the pure segmental relaxation, i.e., α-relaxation, and the second process, at higher temperatures, the α_c-relaxation. Similar behavior is seen for PDMSlin380. For both samples, the relaxation peaks can be well described by the empirical Havriliak−Negami function, as illustrated in Figure 2.

Since the relaxation peak represents a kind of a distribution of relaxation times, it is convenient to normalize the peaks, to get information about temperature-dependent changes on the peak shape. While the shape of the relaxation peak for the PDMS-g-PDMS bottlebrush polymer, belonging to the pure α-relaxation, does not change with temperature (Figure 3), those of the α_c-relaxation narrows with increasing temperature (inset Figure 3).

The same behavior is also seen for our PDMSlin380k sample (Supporting Information, Figure S7) and, additionally, for different molecular weights of linear PDMS, as reported by Hintermeyer et al.[34] Therefore, the distribution of relaxation times stays the same over the entire temperature range of the α-relaxation, independent of the architecture. To compare the

https://dx.doi.org/10.1021/acs.macromol.0c02104
Macromolecules 2021, 54, 1829−1837

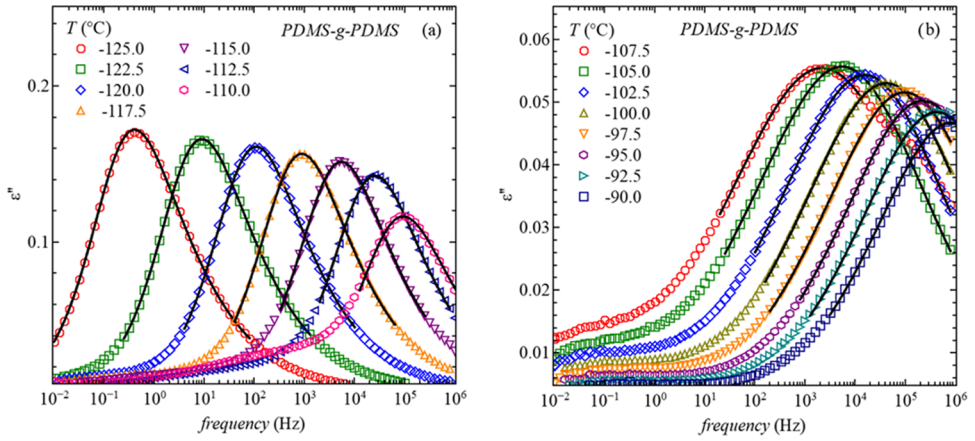

Figure 2. Dielectric permittivity, ε'', vs frequency for the PDMS-g-PDMS bottlebrush polymer for (a) α-relaxation and (b) α_c-relaxation. The solid lines are the best description with the HN function.

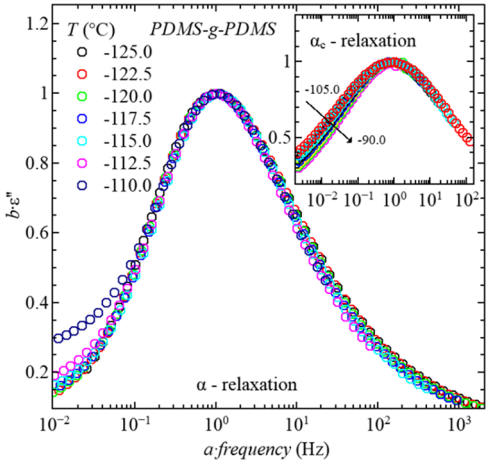

Figure 3. Normalized dielectric permittivity, $b{\cdot}\varepsilon''$, vs normalized frequency for the α-relaxation and the α_c-relaxation (inset). The slightly increased ε'' at low frequencies of $T = -110.0$ °C indicates the emergence of the α_c-relaxation in the frequency window.

shape of the two samples more easily, we are concentrating on the shape parameters β and γ, which give information about the asymmetric broadening of the relaxation peak. Hereby, the value of β describes the low and the product of $(\gamma{\cdot}\beta)$ those for the high-frequency region. As seen in Figure 4a, the values of the high-frequency side are very similar for both architectures and seem to be constant over the entire temperature range. This is consistent with the temperature-independent shape of the relaxation peak, as illustrated in Figure 3. However, concentrating on the β parameter, i.e., the low-frequency side, we have constant but different values for the two architectures. In the case of the PDMSlin380k, the values are smaller compared to those for the bottlebrush. This implies a broader relaxation peak and thus a broader distribution of relaxation times for the PDMSlin380k (Supporting Information, Figure S8).

Focusing on the α_c-relaxation as illustrated in the inset of Figure 3 for the bottlebrush polymer, a narrowing occurs with increasing temperature. This implies a slight increase of the β values, as seen in Figure 4b. In the case of PDMSlin380k, the narrowing is less pronounced, and therefore, the β values are almost independent of the temperature (Figure 4c). The shape of the high-frequency side does not change with temperature and therefore shows constant values, i.e., $\gamma{\cdot}\beta \approx$ const. for both samples. The effect responsible for the α_c-relaxation is known as the cold crystallization and not only shows a temperature-dependent shape change but also a time dependent one, as seen in the Supporting Information, Figure S6 or by Lund et al.[33]

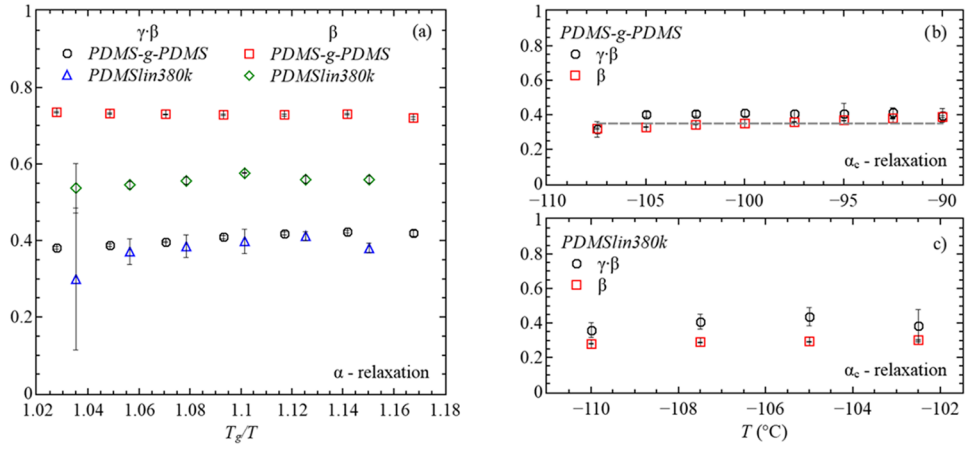

Figure 4. Temperature dependence of the shape parameters, β and γ, resulting from the Havriliak–Negami fitting function for (a) α-relaxation; (b, c) α_c-relaxation. The gray dashed line in (b) is a guide for the eye.

https://dx.doi.org/10.1021/acs.macromol.0c02104
Macromolecules 2021, 54, 1829–1837

Another way to compare these two samples is by focusing on the temperature behavior of the relaxation times, τ_s, as illustrated in Figure 5. Clearly, the two processes, at low (α-relaxation) and high temperatures (α_c-relaxation) are well distinguishable. With increasing temperature, the relaxation times decrease and at a certain temperature, the second process takes over and prevails the measured signal.

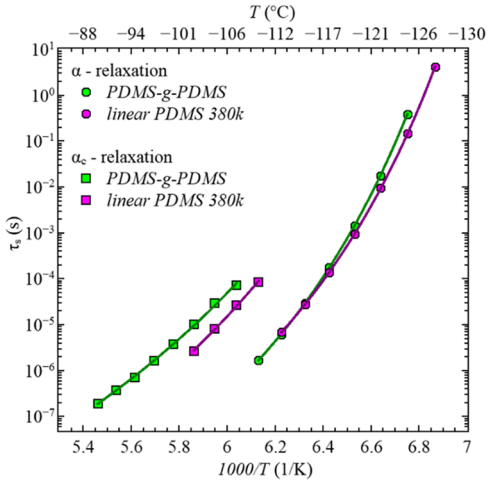

Figure 5. Relaxation times, τ_s, vs $1000/T$, for the PDMS-g-PDMS bottlebrush polymer and PDMSlin380k. The solid lines are the best description with the VFT equation. Errors are within symbol size and omitted.

At very low temperatures, slight deviation between the PDMS-g-PDMS bottlebrush and the PDMSlin380k sample is visible, while with increasing temperature, the relaxation times of both samples become more similar and ultimately show an almost overlapping temperature dependence in the region of $T \sim -120$ °C to $T \sim -110$ °C. The different relaxation times at low temperature are most likely routed in the slightly different glass transition temperatures, T_g, determined as $T_g = T(\tau_s = 100$ s) and additionally by differential scanning calorimetry (DSC) measurements (Table 2) (related data are in Supporting Information, Figures S4 and S5).[20] Hereby, the difference of around $\Delta T_g \sim 10$ °C seems plausible and is related to the heating/cooling rate. While for fast heating/cooling rates, the glass transition temperature shows higher values, and those for slow heating/cooling rates values are lower.[35] In the case of DSC, a rate of 10 °C/min was used during the heating cycle. For dielectric spectroscopy, the heating rate on average is much lower since one isothermal scan takes around 45 min. Therefore, DSC uses a higher heating/cooling rate compared to dielectric spectroscopy and thus results in higher values for T_g, as seen in Table 2.

After the pure segmental relaxation, the α_c-relaxation sets in, with different relaxation times related to the different architectures. Here, the bottlebrush sample has longer relaxation times compared to the linear polymer. This might be due to the molecular weight and an architectural dependent smaller extent of crystallization of PDMS. Hereafter, we are only focusing on the pure segmental relaxation, i.e., α-relaxation.

For both samples, the temperature dependence of the relaxation times can be well described by the Vogel−Fulcher−Tammann (VFT) equation (eq 6). The resulting fit parameters for the description of the α-relaxation are summarized in Table 3 and for the α_c-relaxation are given in Table S1 (Supporting Information).

Table 3. Resulting Fit Parameters for the Temperature Dependence of the Relaxation Times of the α-Relaxation, Described with the VFT Equation and Glass Transition Temperature Determined by Dielectric Spectroscopy (DS) and Differential Scanning Calorimetry (DSC) Measurements

	PDMS-g-PDMS	PDMSlin380k
τ_∞ (s)	$(1.1 \pm 0.2) \times 10^{-14}$	$(3.9 \pm 1.2) \times 10^{-14}$
A (K)	(715 ± 10)	(690 ± 17)
T_0 (K)	(125.3 ± 0.2)	(124.3 ± 0.3)
T_g (°C) [DS]	(-128.4 ± 0.1)	(-129.4 ± 0.4)
T_g (°C) [DSC]	−120.2	−119.3

Large-Scale Polymer Dynamics—FFC-NMR. Since dielectric spectroscopy (DS) only detects the segmental dynamics in the case of PDMS, we have used fast field cycling (FFC) NMR to get information about the polymer dynamics of both samples. Hereby, the measured quantity is the frequency-dependent relaxation rate, $R_1(\omega)$, which can be transformed into the susceptibility representation via $\chi''(\omega) = \omega R_1(\omega)$ to create susceptibility master curves as seen in Figure 6. The frequency-dependent susceptibilities for different temperatures can be found in the Supporting Information, Figure S9.

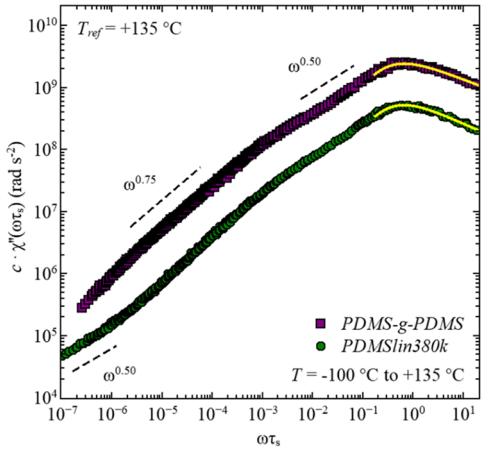

Figure 6. Susceptibility master curve, $\chi''(\omega\tau_s)$, vs normalized frequency, $\omega\tau_s$, for PDMS-g-PDMS and PDMSlin380k at the reference temperature, $T_{ref} = +135$ °C, composed of values from $T = -100$ °C to $T = +135$ °C. The yellow solid lines are the best description with the combination of Cole−Davidson functions (eq 9); the dashed lines represent the resulting power laws. PDMSlin380k data are shifted by a factor $c = 1/5$ for clarity reason.

Both master curves show a well-pronounced peak at high frequencies, followed by a slight shoulder and power laws by going to low frequencies. This slight shoulder in the region of $10^{-3} < \omega\tau_s < 10^{-1}$ comes along with a power law of $\omega^{0.5}$ at the high-frequency side and transitions to a power low of $\omega^{0.75}$ at low frequencies. This behavior is typical for linear PDMS, however, rather unusual for other polymers.[25,36] This originates from the interplay between intra- and intermolecular interactions. For PDMS, the intermolecular contributions are dominating, starting at $\omega\tau_s \approx 10^{-1}$. In the region of the relaxation peak, $\omega\tau_s \approx 1$, both contributions, inter- and

https://dx.doi.org/10.1021/acs.macromol.0c02104
Macromolecules 2021, 54, 1829−1837

intramolecular, have basically the same amplitude. Therefore, the shoulder can be seen as a crossover between inter- and intramolecular relaxation.[25]

The region of the power law $\omega^{0.75}$ belongs to the chain dynamics and fulfills the theoretical expectation for linear PDMS, independent of the molecular weight and architecture, whereas the power law $\omega^{0.5}$, at higher frequencies, agrees with the value observed for high-molecular-weight linear PDMS.[37,38] In this particular region, the literature assumes an interplay of glassy and polymer dynamics.

In the case of PDMSlin380k, an additional power law, $\omega^{0.5}$, at very low frequencies is present, which is absent in the data of the bottlebrush sample. This behavior indicates entanglements that are missing in the bottlebrush polymer results.[36,38]

The relaxation peak is associated with the segmental relaxation time, τ_s, suitable for the specific reference temperature, T_{ref}. Equation 9 allows extracting τ_{CD} that transforms into τ_s using eq 10. With the shift parameters, used for creating the susceptibility master curve, the relaxation times for each respective temperature can be determined.

In case of PDMSlin380k, it was impossible to measure suitable temperatures for the relaxation peak due to fast crystallization. Therefore, data from a linear PDMS with M_n = 2600 g/mol were measured and taken for the relaxation peak only. Based on literature, the peak itself is not influenced by different molecular weights of linear PDMS.[36] In contrast, for the PDMS-g-PDMS bottlebrush polymer, the crystallization was minimized by quenching the sample prior to the measurement scans. Here, there is no signature of crystallization during the measurement.

As seen in Figure 7, the relaxation times for the α-relaxation obtained by FFC-NMR can be well combined with those from dielectric spectroscopy.

While slight differences occur at low temperatures, at high temperatures, both samples coincide. With increasing temperature, the decay of the relaxation times slows down due to a saturation effect, occurring at infinite temperatures. This ability of combing the relaxation times from FFC-NMR and dielectric spectroscopy extends the assumption of a molecular weight as well as architectural-independent segmental relaxation up to high temperatures.

Since Figure 6 already indicates missing entanglement effects for the bottlebrush polymer, focusing on the mean square displacement is appropriate to distinguish different relaxation processes occurring in the available time scale. Hereby, eq 11 is used resulting in the segmental mean square displacement, illustrated for both samples in Figure 8.[24,26]

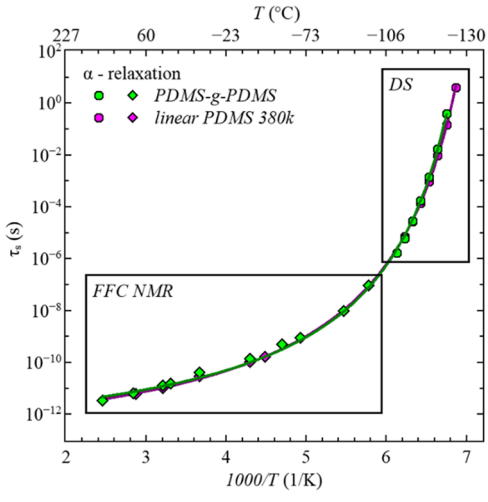

Figure 7. Relaxation time, τ_s, vs $1000/T$, for PDMS-g-PDMS and PDMSlin380k by FFC-NMR (high temperatures) and dielectric spectroscopy (low temperatures). The solid lines are a combined description of FFC-NMR and dielectric spectroscopy (DS) with the VFT equation. The black boxes indicate the different regions resulting from the different instruments. Standard deviations are within symbol size and omitted.

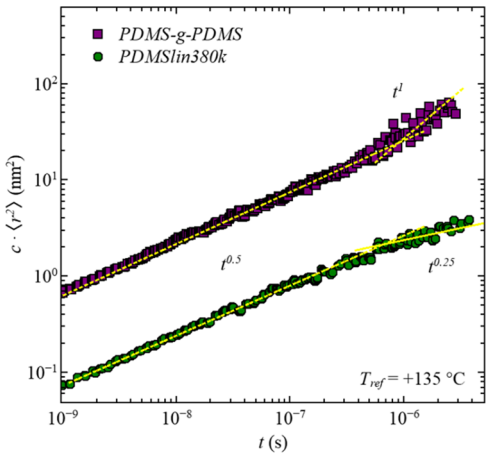

Figure 8. Mean square displacement, $\langle r^2(t)\rangle$, vs time, t, of PDMS-g-PDMS and PDMSlin380k at T_{ref} = +135 °C. The dashed lines are the evolving power laws, associated with different regimes of the polymer dynamics. The PDMSlin380k data are shifted by a factor c = 0.1 for clarity.

In both polymers, two different power law regimes exist. At short times, both polymers show the same power law of $t^{0.5}$, suggesting Rouse dynamics. While the bottlebrush continues with a power law of t^1 indicative for diffusion, starting at τ_R = 900 ns, PDMSlin380k shows a power law of $t^{0.25}$ starting at t = 600 ns. This regime denotes the constraint Rouse regime. Continuing to longer times would result in reptation, $\langle r^2(t)\rangle \propto t^{0.5}$, and finally diffusion, $\langle r^2(t)\rangle \propto t^1$.

The regime of constraint Rouse dynamics is only accomplished by polymers with high molecular weight, where entanglement effects are present. This comparison shows that even if the PDMS-g-PDMS bottlebrush polymer has a high overall molecular weight, the dynamics pursue still the trends of low-molecular-weight linear PDMS with no entanglement effect and pure Rouse dynamics until the onset of diffusion. Similar results are reported by Hu et al. for bottlebrush polymers with polynorbornene and polylactide side chains.[8] Additionally, this is accompanied by a shift of the entanglement molecular weight to higher values, simply by attaching side chains to a linear backbone, as suggested by rheology measurements.[39] Since the dynamics probed by FFC-NMR are mainly governed by the side chains, it can also be seen as a comparison of a linear PDMS with $M_n^{\text{side chain}}$ = 8100 g/mol fixed at one end with a linear PDMS with M_n = 370 000 g/mol. Using this approach, it is not uncommon to see these two different relaxation behaviors based on the large-scale chain dynamics.

https://dx.doi.org/10.1021/acs.macromol.0c02104
Macromolecules 2021, 54, 1829−1837

SUMMARY AND CONCLUSIONS

We have studied two PDMS-based samples, having similar molecular weight, M_n, but significantly different architectures, i.e., spherical bottlebrush vs linear, to investigate how the dynamical behavior is influenced by structural changes. The melt morphology of the bottlebrush sample was examined by small-angle neutron scattering resulting in a spherical form factor, including the description of the internal chain structure of the side chains. For dynamical studies, a combination of dielectric spectroscopy and fast field cycling NMR was used to cover the time scales from segmental relaxation up to large-scale polymer dynamics. Hereby, the segmental dynamics show architectural independence, whereby the large-scale polymer dynamics depends substantially on it. While the bottlebrush polymer pursues Rouse dynamics followed by diffusion, PDMSlin380k shows pronounced entanglement effects. Therefore, even if the molecular weights are similar, remarkable differences related to the different polymer conformation occur in the polymer dynamics despite architectural independence of the segmental relaxation.

ASSOCIATED CONTENT

Supporting Information

The Supporting Information is available free of charge at https://pubs.acs.org/doi/10.1021/acs.macromol.0c02104.

Gel-permeation chromatography (GPC) description and results, nuclear magnetic resonance (NMR) spectroscopy results, differential scanning calorimetry (DSC) experiment description and results, normalized dielectric spectroscopy data for PDMSlin380k, the comparison of normalized dielectric spectroscopy data of PDMS-g-PDMS and PDMSlin380k, fit parameter for describing the temperature dependence of the α_c-relaxation, and the frequency-dependent susceptibilities for different temperatures (PDF)

AUTHOR INFORMATION

Corresponding Authors

Karin J. Bichler − *Department of Physics and Astronomy, Louisiana State University, Baton Rouge, Louisiana 70803, United States;* orcid.org/0000-0002-8666-1859; Email: kbichler@lsu.edu

Gerald J. Schneider − *Department of Physics and Astronomy and Department of Chemistry, Louisiana State University, Baton Rouge, Louisiana 70803, United States;* orcid.org/0000-0002-5577-9328; Email: gjschneider@lsu.edu

Author

Bruno Jakobi − *Department of Chemistry, Louisiana State University, Baton Rouge, Louisiana 70803, United States;* orcid.org/0000-0003-1171-9486

Complete contact information is available at: https://pubs.acs.org/10.1021/acs.macromol.0c02104

Notes

The authors declare no competing financial interest.

ACKNOWLEDGMENTS

The authors acknowledge funding by the U.S. Department of Energy (DoE) under grant DE-SC0019050 and the support of the National Institute of Standards and Technology, U.S. Department of Commerce, in providing the neutron research facility used in this work. The authors are grateful for the support during the SANS beamtime from Elizabeth Kelley. The authors would like to thank ISIS Neutron and Muon source for the DSC measurements, especially Victoria García Sakai, Ian Silverwood, and Cameron Twigg.

REFERENCES

(1) Giussi, J. M.; Azzaroni, O.; Hensel-Bielowka, S.; Wojnarowska, Z.; Knapik, J.; Paluch, M. Synthesis, Characterization and Dielectric Relaxation Study of Hyperbranched Polymers with Different Molecular Architecture. *Polymer* **2016**, *100*, 227−237.

(2) Pyckhout-Hintzen, W.; Allgaier, J.; Richter, D. Recent Developments in Polymer Dynamics Investigations of Architecturally Complex Systems. *Eur. Polym. J.* **2011**, *47*, 474−485.

(3) Kisliuk, A.; Ding, Y.; Hwang, J.; Lee, J. S.; Annis, B. K.; Foster, M. D.; Sokolov, A. P. Influence of Molecular Architecture on Fast and Segmental Dynamics and the Glass Transition in Polybutadiene. *J. Polym. Sci., Part B: Polym. Phys.* **2002**, *40*, 2431−2439.

(4) Jakobi, B.; Bichler, K. J.; Sokolova, A.; Schneider, G. J. Dynamics of PDMS-g-PDMS Bottlebrush Polymers by Broadband Dielectric Spectroscopy. *Macromolecules* **2020**, *53*, 8450−8458.

(5) Bichler, K. J.; Jakobi, B.; Huber, S. O.; Gilbert, E. P.; Schneider, G. J. Structural Analysis of Ultrasoft PDMS-g-PDMS Shell-Only Particles. *Macromolecules* **2020**, *53*, 78−89.

(6) Pesek, S. L.; Li, X.; Hammouda, B.; Hong, K.; Verduzco, R. Small-Angle Neutron Scattering Analysis of Bottlebrush Polymers Prepared via Grafting-through Polymerization. *Macromolecules* **2013**, *46*, 6998−7005.

(7) Rathgeber, S.; Pakula, T.; Wilk, A.; Matyjaszewski, K.; Beers, K. L. On the Shape of Bottle-Brush Macromolecules: Systematic Variation of Architectural Parameters. *J. Chem. Phys.* **2005**, *122*, No. 124904.

(8) Hu, M.; Xia, Y.; McKenna, G. B.; Kornfield, J. A.; Grubbs, R. H. Linear Rheological Response of a Series of Densely Branched Brush Polymers. *Macromolecules* **2011**, *44*, 6935−6943.

(9) López-Barrón, C. R.; Brant, P.; Eberle, A. P. R.; Crowther, D. J. Linear Rheology and Structure of Molecular Bottlebrushes with Short Side Chains. *J. Rheol.* **2015**, *59*, 865−883.

(10) Haugan, I. N.; Maher, M. J.; Chang, A. B.; Lin, T.-P.; Grubbs, R. H.; Hillmyer, M. A.; Bates, F. S. Consequences of Grafting Density on the Linear Viscoelastic Behavior of Graft Polymers. *ACS Macro Lett.* **2018**, *7*, 525−530.

(11) Mijović, J.; Sun, M.; Pejanović, S.; Mays, J. W. Effect of Molecular Architecture on Dynamics of Multigraft Copolymers: Combs, Centipedes, and Barbwires. *Macromolecules* **2003**, *36*, 7640−7651.

(12) Lee, S.; Spencer, N. D. Sweet, Hairy, Soft, and Slippery. *Science* **2008**, *319*, 575.

(13) Pakula, T.; Zhang, Y.; Matyjaszewski, K.; Lee, H.-i.; Boerner, H.; Qin, S.; Berry, G. C. Molecular Brushes as Super-Soft Elastomers. *Polymer* **2006**, *47*, 7198−7206.

(14) Chremos, A.; Douglas, J. F. A Comparative Study of Thermodynamic, Conformational, and Structural Properties of Bottlebrush with Star and Ring Polymer Melts. *J. Chem. Phys.* **2018**, *149*, No. 044904.

(15) Dalsin, S. J.; Hillmyer, M. A.; Bates, F. S. Linear Rheology of Polyolefin-Based Bottlebrush Polymers. *Macromolecules* **2015**, *48*, 4680−4691.

(16) Dalsin, S. J.; Hillmyer, M. A.; Bates, F. S. Molecular Weight Dependence of Zero-Shear Viscosity in Atactic Polypropylene Bottlebrush Polymers. *ACS Macro Lett.* **2014**, *3*, 423−427.

(17) Lee, J. H.; Fetters, L. J.; Archer, L. A. Stress Relaxation of Branched Polymers. *Macromolecules* **2005**, *38*, 10763−10771.

(18) Bichler, K. J.; Jakobi, B.; Sakai, V. G.; Klapproth, A.; Mole, R. A.; Schneider, G. J. Short-Time Dynamics of PDMS-g-PDMS Bottlebrush Polymer Melts Investigated by Quasi-Elastic Neutron Scattering. *Macromolecules* **2020**, *53*, 9553−9562.

(19) López-Barrón, C. R.; Hagadorn, J. R. Dynamic Fragility of α-Olefin Molecular Bottlebrushes. *J. Polym. Sci., Part B: Polym. Phys.* **2019**, *57*, 1293−1299.
(20) Kremer, F.; Schönhals, A. *Broadband Dielectric Spectroscopy*; Springer: Berlin, 2012.
(21) Higgins, J. S.; Benoit, H. C.; Benoît, H. *Polymers and Neutron Scattering*; Clarendon Press, 1996.
(22) Kremer, F. Broadband Dielectric Spectroscopy to Study the Molecular Dynamics of Polymers Having Different Molecular Architectures. In *Physical Properties of Polymers Handbook*; Mark, J. E., Ed.; Springer: New York, NY, 2007; pp 385−393.
(23) Gerstl, C.; Schneider, G. J.; Pyckhout-Hintzen, W.; Allgaier, J.; Richter, D.; Alegría, A.; Colmenero, J. Segmental and Normal Mode Relaxation of Poly(alkylene oxide)s Studied by Dielectric Spectroscopy and Rheology. *Macromolecules* **2010**, *43*, 4968−4977.
(24) Kimmich, R. *Field-Cycling NMR Relaxometry: Instrumentation, Model Theories and Applications*; Royal Society of Chemistry, 2018.
(25) Herrmann, A.; Kresse, B.; Wohlfahrt, M.; Bauer, I.; Privalov, A. F.; Kruk, D.; Fatkullin, N.; Fujara, F.; Rössler, E. A. Mean Square Displacement and Reorientational Correlation Function in Entangled Polymer Melts Revealed by Field Cycling ^{1}H and ^{2}H NMR Relaxometry. *Macromolecules* **2012**, *45*, 6516−6526.
(26) Kresse, B.; Hofmann, M.; Privalov, A. F.; Fatkullin, N.; Fujara, F.; Rössler, E. A. All Polymer Diffusion Regimes Covered by Combining Field-Cycling and Field-Gradient ^{1}H NMR. *Macromolecules* **2015**, *48*, 4491−4502.
(27) Glinka, C. J.; Barker, J. G.; Hammouda, B.; Krueger, S.; Moyer, J. J.; Orts, W. J. The 30 M Small-Angle Neutron Scattering Instruments at the National Institute of Standards and Technology. *J. Appl. Crystallogr.* **1998**, *31*, 430−445.
(28) Kline, S. R. Reduction and Analysis of Sans and Usans Data Using Igor Pro. *J. Appl. Crystallogr.* **2006**, *39*, 895−900.
(29) Dozier, W. D.; Huang, J. S.; Fetters, L. J. Colloidal Nature of Star Polymer Dilute and Semidilute Solutions. *Macromolecules* **1991**, *24*, 2810−2814.
(30) Daoud, M.; Cotton, J. P. Star Shaped Polymers: A Model for the Conformation and Its Concentration Dependence. *J. Phys. France* **1982**, *43*, 531−538.
(31) Utracki, L. A.; Wilkie, C. A. *Polymer Blends Handbook.*; Springer: Netherlands, 2014.
(32) Nagy, E. Chapter 18—Membrane Gas Separation. In *Basic Equations of Mass Transport through a Membrane Layer*, 2nd ed.; Nagy, E., Ed.; Elsevier, 2019; pp 457−481.
(33) Lund, R.; Alegria, A.; Goitandia, L.; Colmenero, J.; González, M. A.; Lindner, P. Dynamical and Structural Aspects of the Cold Crystallization of Poly (dimethylsiloxane)(PDMS). *Macromolecules* **2008**, *41*, 1364−1376.
(34) Hintermeyer, J.; Herrmann, A.; Kahlau, R.; Goiceanu, C.; Rössler, E. A. Molecular Weight Dependence of Glassy Dynamics in Linear Polymers Revisited. *Macromolecules* **2008**, *41*, 9335−9344.
(35) Wrana, C. *Polymerphysik: Eine Physikalische Beschreibung Von Elastomeren Und Ihren Anwendungsrelevanten Eigenschaften*; Springer: Berlin, 2014.
(36) Hofmann, M.; Herrmann, A.; Abou Elfadl, A.; Kruk, D.; Wohlfahrt, M.; Rössler, E. A. Glassy, Rouse, and Entanglement Dynamics as Revealed by Field Cycling ^{1}H NMR Relaxometry. *Macromolecules* **2012**, *45*, 2390−2401.
(37) Kariyo, S.; Brodin, A.; Gainaru, C.; Herrmann, A.; Hintermeyer, J.; Schick, H.; Novikov, V. N.; Rössler, E. A. From Simple Liquid to Polymer Melt. Glassy and Polymer Dynamics Studied by Fast Field Cycling NMR Relaxometry: Rouse Regime. *Macromolecules* **2008**, *41*, 5322−5332.
(38) Herrmann, A.; Kariyo, S.; Abou Elfadl, A.; Meier, R.; Gmeiner, J.; Novikov, V. N.; Rössler, E. A. Universal Polymer Dynamics Revealed by Field Cycling ^{1}H NMR. *Macromolecules* **2009**, *42*, 5236−5243.
(39) Daniel, W. F.; Burdynska, J.; Vatankhah-Varnoosfaderani, M.; Matyjaszewski, K.; Paturej, J.; Rubinstein, M.; Dobrynin, A. V.; Sheiko, S. S. Solvent-Free, Supersoft and Superelastic Bottlebrush Melts and Networks. *Nat. Mater.* **2016**, *15*, 183−189.

https://dx.doi.org/10.1021/acs.macromol.0c02104
Macromolecules 2021, 54, 1829−1837